Investigation of the physical properties of ion assisted ZrN thin films deposited by RF magnetron sputtering

2010 J. Phys. D: Appl. Phys. 43 225401

(http://iopscience.iop.org/0022-3727/43/22/225401)

J. Phys. D: Appl. Phys. **43** (2010) 225401 (8pp) doi:10.1088/0022-3727/43/22/225401

Investigation of the physical properties of ion assisted ZrN thin films deposited by RF magnetron sputtering

M A Signore, D Valerini, A Rizzo, L Tapfer, L Capodieci and A Cappello

ENEA, Department of Physical Technologies and New Materials, SS7, Appia, km 706, 72100 Brindisi, Italy

Received 19 January 2010, in final form 21 April 2010
Published 18 May 2010
Online at stacks.iop.org/JPhysD/43/225401

Abstract

Ion bombardment during thin film growth is known to cause structural and morphological changes in the deposited films, thus affecting their physical properties. In this work zirconium nitride films have been deposited by the ion assisted magnetron sputtering technique. The ion energy is controlled by varying the voltage applied to the substrate in the range 0–25 V. The deposited ZrN films are characterized for their structure, surface roughness, oxygen contamination, optical reflectance and electrical resistivity. With increasing substrate voltage crystallinity of the films is enhanced with a preferential orientation of the ZrN grains having the (1 1 1) axis perpendicular to the substrate surface. At the same time, a decrease in electrical resistivity and oxygen contamination content is observed up to 20 V. A higher substrate voltage (25 V) causes an inversion in the observed experimental trends. The role of oxygen contamination decrease and generation of nitrogen vacancies due to ionic assistance have been considered as a possible explanation for the experimental results.

Introduction

The properties of thin films grown by physical vapour deposition (PVD) processes strongly depend on the energy of the incident particles transferred to the surface of the growing films [1]. This energy available on the surface of the films can promote many phenomena such as the enhancement of surface atom mobility [2], modification of crystallinity [3], variation in composition [4], structure and microstructure and, as a consequence, in the physical response of the deposited material. Ion bombardment permits one to obtain denser and void-free films [5] even by performing a low temperature deposition process which is sometimes more convenient and advantageous [6]. The simplest way to achieve ion bombardment on a growing film during a plasma growth process is biasing the substrate during the deposition. The bias voltage applied to the substrate attracts ions (argon and nitrogen) out from the plasma towards the substrate by the potential drop in the sheath region. At a fixed process total pressure, the energy of these ions [7] will be proportional to this voltage. For small bias voltages, the sheath at the substrate will be thin enough so that it will be collision free [8]. In this investigation the RF reactive magnetron sputtering process was used to grow thin films of ZrN, a material which has been stimulating remarkable scientific interest for its wide field of applications [9]. During the deposition process the total pressure of the reactive gas mixture, the substrate temperature and the power applied to the Zr target were kept constant, while a negative bias voltage was applied to the substrate in the range 0–25 V. A (1 1 1) texture was obtained for the ZrN films and a low electrical resistivity ($\sim$160 $\mu\Omega$ cm) was achieved for the 20 V-biased sample. The role of oxygen and of nitrogen vacancies has been qualitatively discussed for the interpretation of experimental results. Therefore, in this work it is shown how the optimization of substrate bias can simultaneously improve the electrical conductivity and texture of ZrN films. The improvement of these two properties makes ZrN a good candidate as diffusion barrier in microelectronics devices where low resistivity and high texturing are required besides good adhesion, chemical inertness with copper and silicon and high thermal stability [10]. An excellent diffusion barrier behaviour has been found for (1 1 1)-oriented ZrN [11] but this orientation has been attained at a high deposition temperature, while in this work the application of a substrate bias leads to high texturing at room temperature.

1. Experimental details

ZrN films were deposited on (1 0 0)-oriented silicon wafers by reactive RF magnetron sputtering in an Ar/N_2 gas mixture. Both gases were 99.999% pure. The working pressure was kept constant at a value of 1.12×10^{-2} Torr and the nitrogen flux percentage in the mixture was fixed at 5%. The power applied to the Zr target during the deposition was 165 W. The distance between the substrates and the target was 70 mm. The substrate temperature was monitored by a thermocouple and was below 70 °C during the whole process. The only tuned process parameter was the negative bias voltage applied to the substrate in the range from 0 to −25 V with respect to the ground. As a simplification, in the text the voltage absolute values will be indicated. Before the deposition of the nitride films, the target was pre-sputtered in argon atmosphere for about half an hour. The films are about 500 nm thick. The thickness was measured using a profilometer (KLA TENCOR) on steps patterned by a solid mask. The morphology and the roughness of the films were investigated by atomic force microscopy (AFM). The AFM measurements were performed with a Nanoscope III from Digital Instruments. Silicon cantilevers with radius less than 10 nm were used as the tip. All the measurements were performed in tapping mode in air. The x-ray diffraction and reflectivity experiments were carried out using an x-ray diffractometer in parallel beam geometry (Philips MPD PW1880, 3 kW generator) optimized for small-angle scattering measurements. For all the measurements Cu Kα radiation ($\lambda_{CuK_\alpha} = 0.154\,186$ nm) was used. The x-ray diffraction measurements were performed under different geometrical configurations, i.e. by performing both θ–2θ scan as well as grazing-incidence (with fixed incidence angle $\omega_i = 1.0°$) measurements. The grazing-incidence x-ray diffraction (GIXRD) measurements were performed by keeping the incident angle ω_i (angle between the incident beam and the sample surface) fixed at 1.0° and recording the scattered x-ray beam by moving the detector and the post-sample flat graphite collimator–monochromator along the goniometer circle in the 2θ range between 10° and 100° with a step size of 0.02°. The θ–2θ scans were measured in the angular 2θ range between 25° and 45° with a step size of 0.01°, because the Bragg peaks in this angular range only were intense enough to be analysed quantitatively. Within the x-ray reflectivity (XRR) regime, we have taken specular (ω,2θ) scans (XSR), in which the grazing angle of incidence of the x-rays is equal to the exit angle (measured 2θ ranges between 0° and 9° with a step size of 0.01°), and transverse ω scans (XDS, diffuse scattering), in which the angular position of slit and detector (2θ angle) was fixed. DC electrical resistivity at room temperature was deduced from sheet resistance measurements using the in-line four probe method. A CARY 500 spectrometer was employed to perform optical reflectance measurements in the range from 200 to 2500 nm. Standard SIMS measurements have been performed by means of a CAMECA ims4f magnetic sector instrument by using Cs^+ primary ions and detecting Zr^+ and MCs^+ (M = O, N) secondary ions [12].

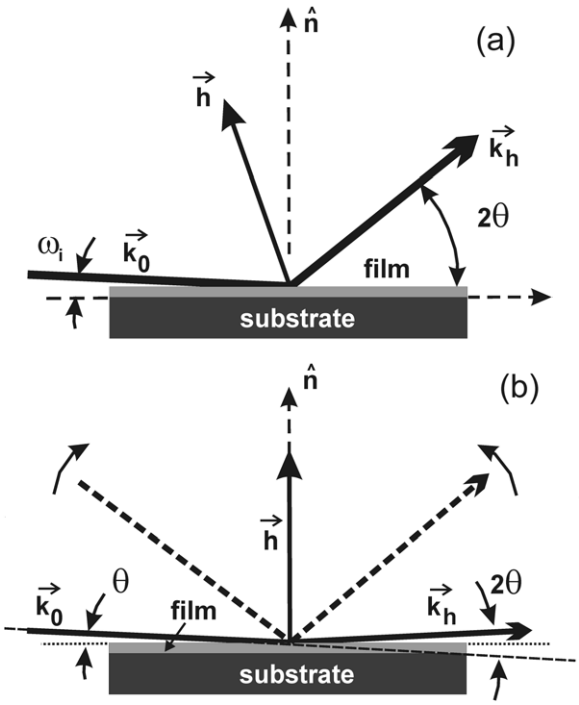

Figure 1. Co-planar x-ray scattering geometries used for the GIXRD (*a*) and XSR (*b*) measurements, respectively. Here, $\boldsymbol{k}_0$ and $\boldsymbol{k}_h$ are the incident and scattered x-ray beams, and $\boldsymbol{h}$ and $\boldsymbol{n}$ are the scattering vector and surface normal, respectively.

2. Results

2.1. Structure and morphology of the films

Generally, for thin films with layer thickness $<1\,\mu$m and nanocrystalline structure GIXRD measurements are more appropriate for a quantitative analysis since the x-ray penetration depth is reduced and the relative Bragg peak intensity is enhanced. The GIXRD and x-ray reflection (XSR) schemes are schematically shown in figure 1. Both measurements are carried out in co-planar scattering geometry. However, in the GIXRD configuration (figure 1(*a*)) the incidence angle ω_i between the incident x-ray beam ($\boldsymbol{k}_0$) and the sample surface is kept constant, while the intensity of the diffracted x-ray beam ($\boldsymbol{k}_h$) is recorded for different 2θ angles. In contrast, for the x-ray specular reflectivity measurements (figure 1(*b*)) the scattered x-ray intensity is recorded keeping the angles between the sample surface and the incident and the reflected x-ray beams, respectively, equal. In this case (*b*), the scattering vector $\boldsymbol{h}$ is parallel to the surface normal $\boldsymbol{n}$. Figure 2 shows the GIXRD patterns of the samples deposited with a negative V_{bias} of 0 V, 10 V and 25 V, respectively, in the 2θ angular range between 10° and 100°. Several Bragg peaks are clearly observed and can be identified in accordance with the PDF 74-1217 [13] of the cubic phase of ZrN. The θ–2θ measurement patterns are shown in figure 3. The 2θ as well the θ–2θ measurements very clearly show that the relative intensity of the (1 1 1) Bragg peaks increases while the width (FWHM) of the (1 1 1) and (2 0 0) Bragg peaks reduces with increasing negative bias voltage V_{bias} applied during sputtering deposition. The average ZrN particle size was estimated from

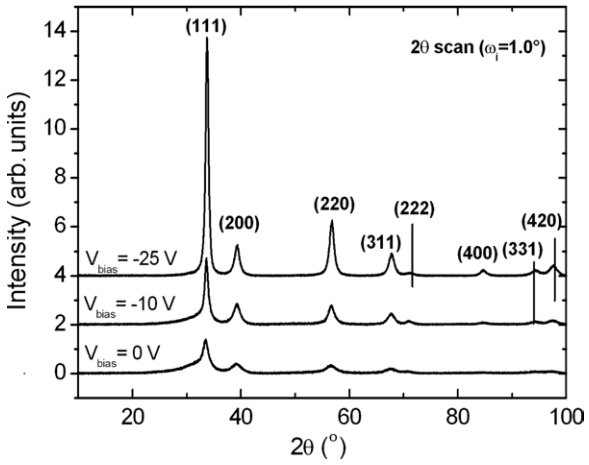

Figure 2. GIXRD measurements (2θ scans) of the same samples deposited under different bias voltage V_{bias} conditions. The Bragg peaks are indexed in accordance with the PDF 74-1217 of the JCDPS-ICDD database and correspond to the c-ZrN ($a_{\text{ZrN}} = 4.63$ Å).

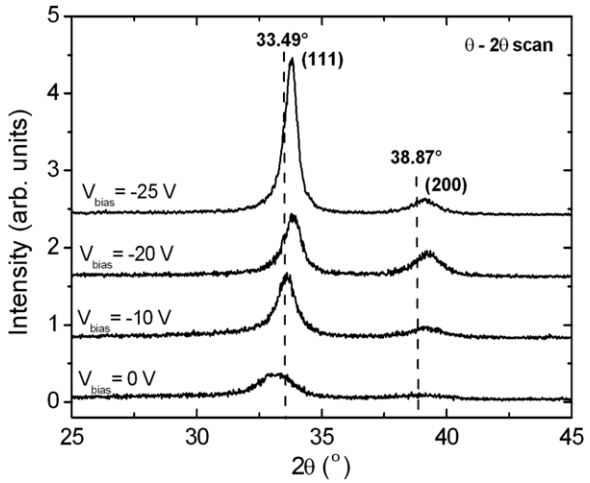

Figure 3. XRD measurements (θ–2θ scans) of samples deposited under different bias voltage V_{bias} conditions. The dashed lines indicate (1 1 1) and (2 0 0) peaks' position according to the PDF 74-1217 card.

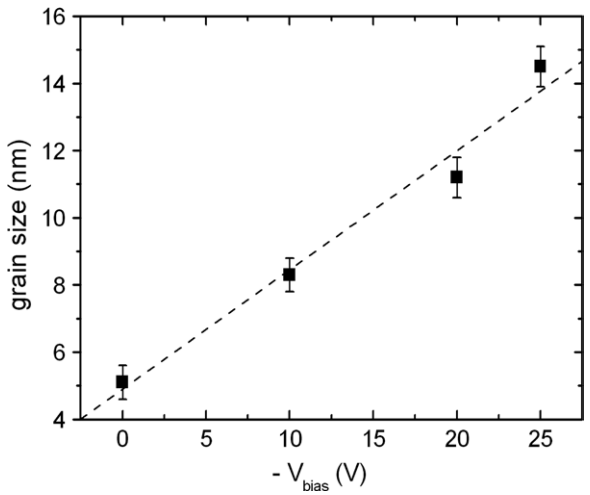

Figure 4. ZrN grain size as a function of the applied bias voltage V_{bias}. An almost linear relationship is observed under the considered experimental conditions.

the broadening of the (1 1 1) and (2 0 0) diffraction peaks by using a Cauchy fit of the peak profiles and applying Scherrer's formula [14]:

$$D = 0.94\lambda/(\Delta\omega \cos\,\theta_{\text{B}}), \tag{1}$$

where D is the average crystallite size, λ is the x-ray wavelength, $\Delta\omega$ is the calculated FWHM of the diffraction peak in radians and θ_{B} is the Bragg angle. The grain size increases linearly with increasing bias voltage V_{bias} starting from 5.1 nm to 14.5 nm, for $V_{\text{bias}} = 0$ V and 25 V, respectively. The results are depicted in figure 4 and summarized in table 1. In addition, the diffraction patterns in figures 2 and 3 show that the relative intensity ratio between the Bragg peaks does not correspond to the expected values as reported in the PDF 74-1217; for example the (2 0 0) Bragg peak intensity should be only slightly lower than the (1 1 1) Bragg peak intensity by about 15%. Furthermore, the relative (1 1 1) peak intensity increases with increasing applied bias voltage V_{bias}. These findings indicate a pronounced extension of the ZrN grains along the (1 1 1) crystallographic axis and a preferential orientation of the ZrN grains having the (1 1 1) axis perpendicular to the substrate surface, i.e. parallel to the deposition/growth direction. This texture of the closest packed plane is the most frequently encountered in fcc structure such as zirconium nitride [15, 16]. A pronounced angular deviation of all the most intense Bragg peaks of the GIXRD as well as the XRD patterns is observed. In particular the angular shift of the (1 1 1) Bragg peak in figure 3 is clearly visible. A reliable and accurate determination of the angular peak positions (by employing a peak profile fitting) is possible only for the most intense Bragg peaks, i.e. the (1 1 1), (2 0 0), (2 2 0) and (3 1 1) peaks. The increase in the angular position of the diffraction peaks with the bias voltage corresponds to a decrease in the lattice constant, whose values were determined from Bragg's law and are reported in figure 5 and in table 1. It should be noted that the value reported for c-ZrN is about 4.63 Å [12]. Specular x-ray reflectivity (XSR) and transverse scan (XDS) measurements were performed in order to investigate the surface morphology, the density and the chemical composition of the deposited ZrN films. Figure 6 shows the XSR and the transverse scans recorded for different 2θ positions of the samples assisted at $V_{\text{bias}} = 0$ V and $V_{\text{bias}} = 10$ V. The XSR patterns show a very fast decay of the reflected intensity above the critical angle. The fast intensity decay observed above the critical angle θ_{c} indicates a high surface roughness ($\geqslant$5 nm); however, its precise value cannot be determined within the Nevot–Croce model that yields reliable data typically for root mean square (RMS) roughness $<$5 nm. The determination of the critical angle values (reported in table 1) through the angular position of the fast intensity decay of the XSR pattern and of the Yoneda peak positions allows us to determine the mass density (or the real part of the dielectric susceptibility) of the deposited ZrN films. The mass density is related to the critical angle θ_{c} by

Table 1. Physical parameters (lattice parameter, grain size, critical angle, mass density) as determined from XRD and XRR measurements and RMS roughness values evaluated by AFM measurements.

	Negative bias voltage V_{bias} (V)	Grain size D (nm) (±0.5)	Lattice parameter c (Å) (±0.0013)	Critical angle θ_c (deg) (±0.007)	Mass density (g cm^{-3})	RMS roughness (nm)
	0	5.1	4.6768	0.30	4.82	5.5
	10	8.3	4.6232	0.32	5.48	6.7
	20	10.2	4.5855	0.335	6.00	10.8
	25	14.5	4.5921	0.35	6.56	10.8
c-ZrN	—	—	4.63	0.364	7.09	—

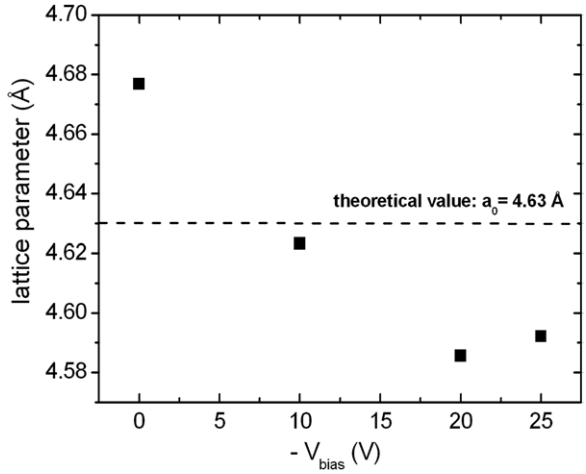

Figure 5. Lattice parameter as a function of the applied negative bias voltage V_{bias}. An almost linear relationship is observed under the considered experimental conditions.

the equation [14]

$$\rho_m = \frac{\pi \cdot \theta_c^2}{r_e \cdot \lambda^2 \cdot N_A} \cdot \frac{\sum_i (Z_i + f_i')}{\sum_i M_i}, \qquad (2)$$

where r_e is the classical electron radius, λ is the x-ray wavelength used, N_A is Avogadro's number, and $Z_i\, f_i'$ and M_i are the nuclear charges, the dispersion corrections and the atomic weights of the ith chemical element, respectively. The mass density of the deposited ZrN films as a function of the applied bias voltage V_{bias} was evaluated using equation (2) and is shown in figure 7 where it is clear that its increase follows the voltage rise.

AFM micrographs (figure 8) give evidence of all the deposited samples' topography. They exhibit a 'cauliflower-like' surface which can be observed when a thin film has a columnar structure with a grain size of tens of nanometres [7], as previously confirmed by XRD analysis (figure 4). The evaluated average RMS roughness is in the range 5–11 nm as reported in the last column of table 1 corroborating XSR results which evaluate surface roughness values higher than 5 nm.

2.2. Optical and electrical analyses

The characteristic feature of the reflectance spectra is a distinct minimum located in the range between 2.8 and 3.5 eV, followed by a sudden rise, the so-called 'plasma reflectance edge' [17], at lower energies (figure 9). The high reflectance in the IR range is related to the high light absorption by the free electron gas (conduction electrons, described by the Drude model), while the reflectance in the UV range is related to the absorption by the interband transitions of the bounded electrons (described by the Lorentz oscillators). As a consequence, the reflectance spectra can be fitted by the use of a model including a Drude part and one or more Lorentz oscillators. The energy of the reflectance minimum, the reflectance percentage at 0.8 eV and the plasma energy of the Drude part are listed in table 2. A detailed analysis of the optical spectra by a Drude–Lorentz model is in progress and it will be reported in a future paper.

The position of the reflectance minimum shifts to higher energy when the voltage increases up to 20 V, then it slightly decreases for the film assisted at 25 V. At the same time, the reflectance in the low energy range also increases with the applied bias voltage until 20 V, and it slightly decreases at 25 V. Both these behaviours are reported in the inset of figure 9. The plasma energy value follows the same trend, as it has an increase until 20 V and a following decrease at 25 V (see table 2).

A similar behaviour can be observed in the electrical measurements too. Indeed the general result obtained by the four-point probe method measurements is that the application of a bias voltage significantly lowers the electrical resistivity down to a minimum value at 20 V, after which an inversion is observed, as reported in figure 10 and in table 2. In particular, the unbiased ZrN film exhibits the highest resistivity value (13 240 $\mu\Omega$ cm) that is lower than the value found by Pilloud *et al* [16] (27 000 $\mu\Omega$ cm) evaluated by the same technique. The lowest resistivity value in our samples is ∼160 $\mu\Omega$ cm, which is comparable to the lowest value found in [15] (∼150 $\mu\Omega$ cm). However it is noteworthy that in our case this low value is obtained at a bias voltage value of 20 V, far lower than that used in [15] (160 V). In the analysed negative bias voltage range (0–25 V) the electrical resistivity of the ZrN films is at least one order of magnitude higher than that of the bulk material (13.6 $\mu\Omega$ cm) [18], as already noted by other authors [19, 20].

2.3. Oxygen contamination: SIMS analysis

Oxygen contamination is the most challenging problem for deposition of films by PVD process, above all for transition metal nitrides due to the strong affinity of the metal to oxygen. To verify the oxygen incorporation, SIMS analysis was performed on all the deposited samples by monitoring

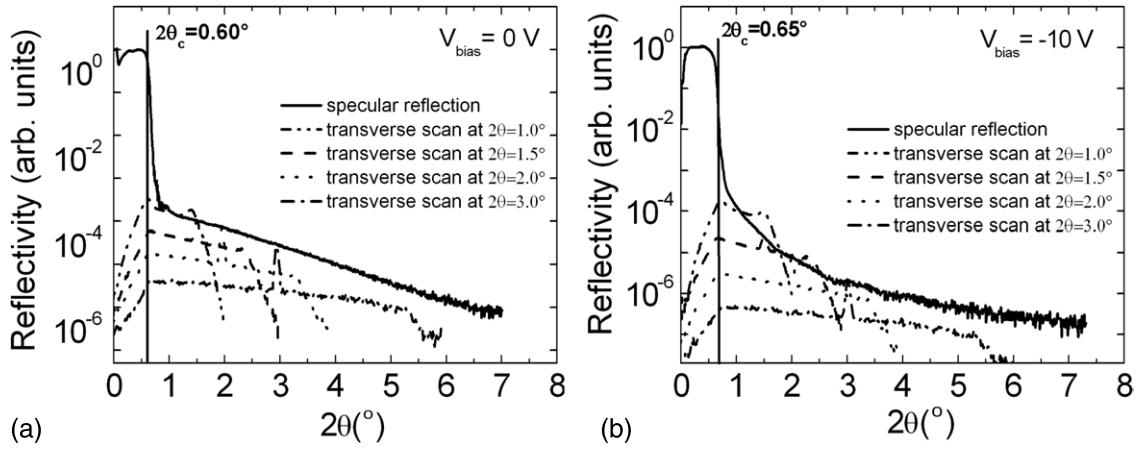

Figure 6. The XSR and the transverse scans recorded for different 2θ angular positions of the samples assisted at $V_{\text{bias}} = 0$ V (*a*) and at $V_{\text{bias}} = 10$ V (*b*). The dashed line indicates the angular position of the critical angle (angular position of the low-angle Yoneda wing).

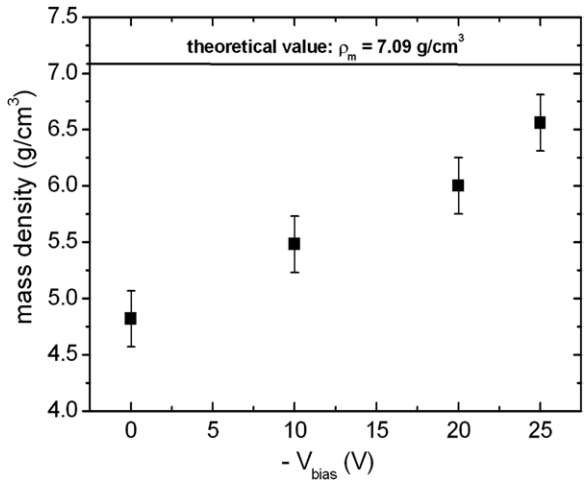

Figure 7. The mass density of the deposited ZrN films increases linearly with increasing applied bias voltage V_{bias}. The theoretical value of c-ZrN mass density is indicated by the line.

the CsO^+ molecular ion. The exact composition cannot be determined by the SIMS measurement due to the lack of a standard reference ZrN material. Therefore, the ratio of the oxygen signal number to the total signal number of the films' elements (Zr, O and N) was calculated as a qualitative indication. In particular these values were normalized with respect to the 20 V-assisted oxygen signal taken as the reference and are reported in figure 11. Although these values do not correspond to the exact chemical composition, it is possible to compare the relative oxygen content in different samples. They indicate that the amount of oxygen is approximately the same in the first three samples (0, 5, 10 V), while it decreases on biasing the substrate at 15 and 20 V, and then it slightly increases again for the sample deposited at 25 V.

3. Discussion

The main remarkable effects related to an increase in the substrate bias voltage observed in our study are a pronounced preferential orientation of the ZrN grains along the (1 1 1) crystallographic axis, an increase in density and grain size of the films, a decrease in lattice parameter and electrical resistivity, a shift of the reflectance minimum towards a higher energy and an increase in the reflectivity percentage in the near infrared region.

The (1 1 1) preferential orientation results from an increase in kinetic energy and momentum of the incident ions with increasing bias voltage at a constant deposition pressure [21], inducing intrinsic compressive stresses in the films through substitution of atoms or generation of vacancies [22]. In this case, the strain energy determines the overall energy of the films, and (1 1 1) would become the preferred orientation to minimize it [23]. It is noteworthy that the bias voltage in our films does not have any significant effect on film adhesion, while higher bias voltages (>25 V) led to some film detachment from the substrate, probably due to the higher intrinsic compressive stress induced in the film.

The observed experimental results can be similarly attributed to two different causes: nitrogen replacement by oxygen or generation of nitrogen vacancies in the ZrN lattice. Indeed, considering the lattice parameter, its decrease to values lower than the bulk one (4.63 Å) on increasing the assistance energy can be ascribed to stress introduced in the lattice due to nitrogen vacancies [24] or to nitrogen substitution by oxygen atoms [25]. In the first case the presence of nitrogen vacancies can influence the film lattice parameter without inducing strong structural alterations: it is known that transition metal nitrides have a vacancy defect structure, which is stable over a wide range of compositions allowing a change in the stoichiometry without altering the NaCl crystal structure [26]. In particular, this has also been noted for nitrogen-deficient ZrN films [27]. In the second case, O atoms presumably tend to substitute N atoms because they are too large to be inserted into the interstitial sites of ZrN lattice causing a decrease in the lattice parameter [28]. For this reason, the examination of the experimental results can help to qualitatively distinguish the respective influence of both factors.

According to the SIMS oxygen signals, the samples can be grouped into three classes: films deposited with V_{bias} in the range 0–10 V (I) where the oxygen content is almost

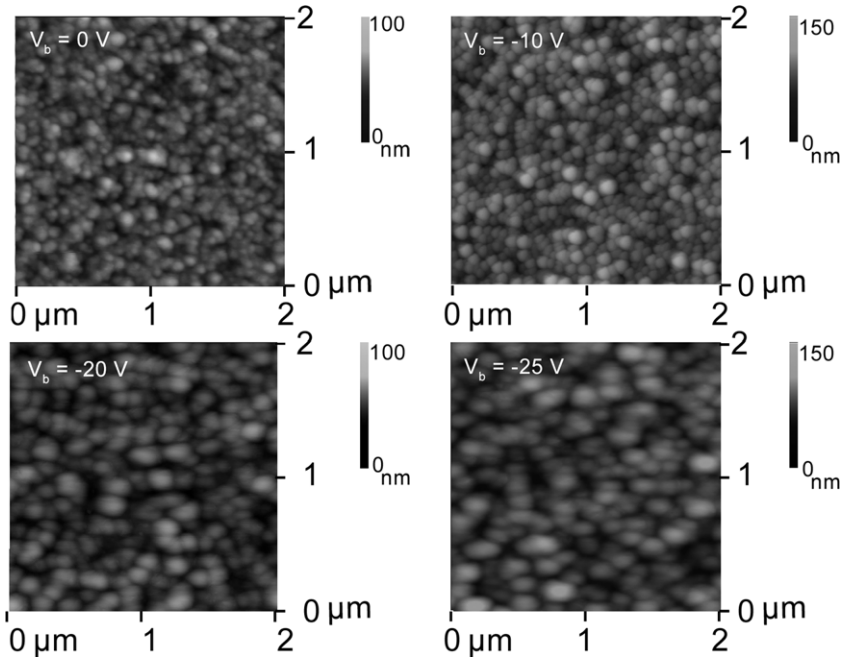

Figure 8. AFM micrographs of the samples deposited at different applied substrate bias voltages as indicated in each picture. The roughness values are calculated on (2 × 2) μm^2 areas.

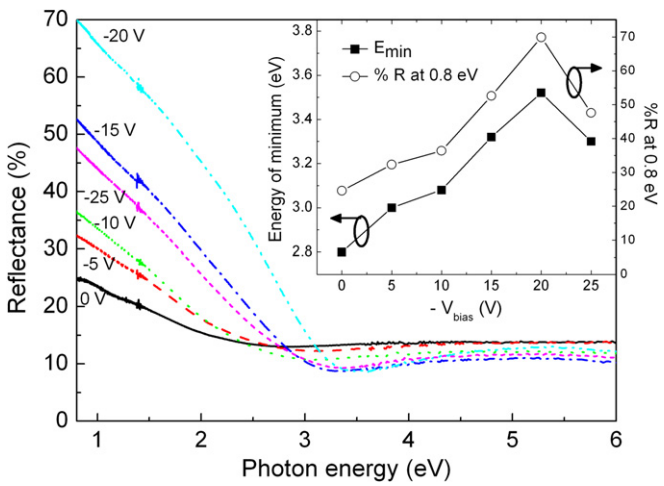

Figure 9. Reflectance spectra of the films deposited at different applied substrate bias voltages. Inset: dependence of the energy of the reflectance minimum (solid squares, left axis) and of the reflectance percentage at 0.8 eV (empty circles, right axis) on the applied bias voltage.

(This figure is in colour only in the electronic version)

the same, the 15 V and 20 V-assisted samples (II) where the contamination content quickly decreases and the 25 V-assisted sample (III) where the oxygen content slightly increases again.

Although the oxygen quantity is the same for the samples belonging to group I, their physical properties significantly change: the crystallinity is enhanced (the FWHM of the ZrN(1 1 1) peak decreases) thanks to the adatom mobility enhancement related to the increased bombardment energy which allows the grain growth and the improvement of films' mass density [29]; the electrical resistivity decreases by about six times changing from 13 240 $\mu\Omega$ cm (0 V) to 2300 $\mu\Omega$ cm

Table 2. Values of the energy of the reflectance minimum, the reflectance percentage at 0.8 eV, the plasma energy and the electrical resistivity as determined by optical and electrical analyses.

$-V_{bias}$ (V)	Energy of the reflectance minimum (eV)	Reflectance percentage at 0.8 eV (%)	Plasma energy (eV)	Resistivity ($\mu\Omega$ cm)
0	2.8	24.6	1.8	13 240
5	3.0	32.3	2.7	4 020
10	3.1	36.4	3.2	2 300
15	3.3	52.6	4.9	296
20	3.5	69.9	6.9	1 59
25	3.3	47.6	4.0	2 80

(10 V); the reflectance minimum shifts by about 0.3 eV to higher energies from 0 V to 10 V; the reflectance percentage in the near infrared region and the plasma energy rise from ∼25% to ∼36% (measured at 0.8 eV) and from 1.8 eV to 3.2 eV, respectively. Since the oxygen content in these films is almost unchanged, these variations can be attributed mainly to the changes in the presence of nitrogen vacancies, probably due to a preferential re-sputtering of nitrogen atoms during the ion assistance. In particular, the non-assisted sample exhibits the highest lattice parameter, even higher than the value in the bulk material, thus suggesting the lowest content of nitrogen vacancies. This is in agreement with the optical and electrical measurements. Indeed the plasma energy is proportional to the square root of the free electron density, therefore the increase in its value and the corresponding shift of the reflectance minimum towards high energies indicate an increase in the free electron density. At the same time the reflectance in the low energy range, related to free electrons, increases when the bias voltage is increased from 0 to 10 V. These observations indicate an increase in the free electron density with the bias voltage, in accordance with the electrical

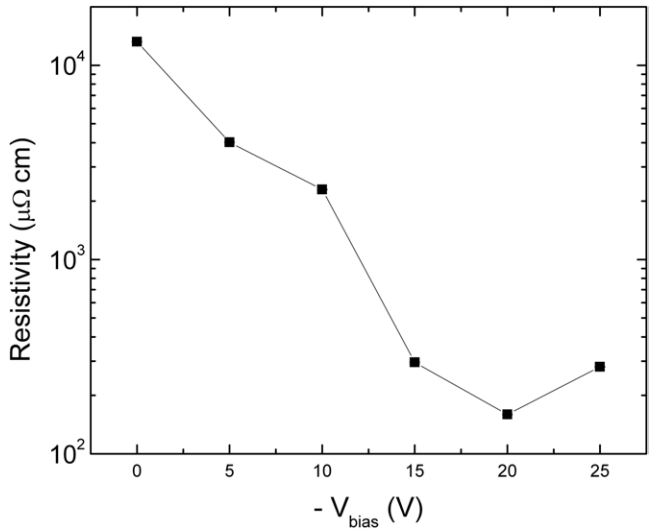

Figure 10. Dependence of the electrical resistivity (log scale) on the substrate bias voltage.

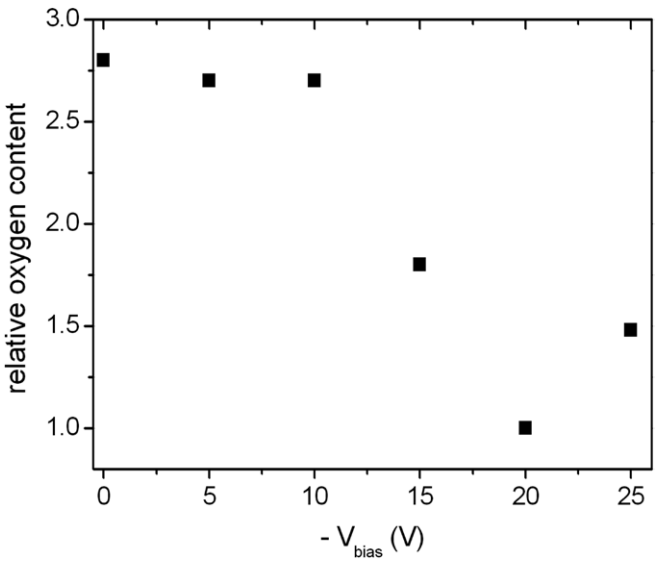

Figure 11. Relative oxygen content versus substrate voltage as derived by SIMS measurements. Each value has been normalized with respect to the signal of the 20 V-assisted sample taken as the reference.

resistivity measurements, showing a decrease in the resistivity. This can be explained considering that the formation of zirconium nitride implies the transfer of electrons from the d-band of zirconium atoms to the p-states of nitrogen ones according to the ionic model of the transition metal nitride [7], and hence a decrease in nitrogen content causes an increase in the number of free electrons supplied by Zr atoms since these electrons are not involved in the bonds with the missing N atoms. As a confirmation, in the literature a shift of the reflectance minimum to high energies has been observed when the nitrogen content in ZrN films is decreased [30].

The decrease in oxygen content in the samples of group II causes an additional increase in the free electron density, thus further inducing a shift of the reflectance minimum (up to 3.5 eV) and an increase in the reflectance intensity in the low energy range (up to ∼70%) and of the plasma energy (almost 7 eV), and a decrease in the electrical resistivity (down to ∼160 $\mu\Omega$ cm). The electrical conductivity is also improved by the decrease in the electron scattering probability due to both the reduction of oxygen impurities and the increase in film mass density with the bias voltage.

The slight inversion in the trend of the optical and electrical measurements observed for the film grown with V_{bias} of 25 V (group III) can be ascribed to two factors: (i) the high energy bombardment can produce structural defects so that the electrons are captured in the defect states, thus inducing a reduction in the free electron density, and consequently a shift of the reflectance minimum to a low energy (3.3 eV), a decrease in the reflectance percentage in the IR range (∼48%) and of the plasma energy (4 eV), and an increase in the electrical resistivity (280 $\mu\Omega$ cm); (ii) the increased bombardment of ions leads to an implantation phenomenon which incorporates oxygen atoms in the films (as shown by the oxygen SIMS signal) causing the same effects mentioned above.

As already mentioned, the electrical behaviour is in agreement with the optical one, since the electrical resistivity follows the same trend of the plasma energy and thus of the free electron density derived from the optical reflectance spectra. Further investigations are in progress in order to better evaluate the dependence of resistivity on the carrier relaxation time, for example due to the grain size.

4. Conclusions

The negative bias voltage applied to the substrate during the sputtering deposition of zirconium nitride films has significant influence on the structural, compositional, electrical and optical properties of the ZrN films. The films exhibit a highly (1 1 1) preferred orientation due to the minimization of the strain energy. The lattice parameter decreases on increasing the bias and this effect can be due to the nitrogen replacement by oxygen or the generation of nitrogen vacancies caused by the ion bombardment. The simultaneous examination of different characterizations (SIMS, optical reflectance and electrical resistance) allowed us to qualitatively discriminate the influence of the two effects. The trends observed in the optical reflectance and electrical resistivity measurements are in agreement with an increase in the content of nitrogen vacancies with increasing bias voltage until 20 V. A minimum resistivity value of ∼160 $\mu\Omega$ cm is obtained for the film deposited with a negative bias voltage of 20 V. The assistance by a higher bias voltage (25 V) is found to cause an inversion in the trends observed in the contamination, optical and electrical film properties.

References

[1] Thiery F, Pauleau Y and Ortega L 2004 *J. Vac. Sci. Technol.* A **22** 30
[2] Alfonso J E, Torres J and Marco J F 2006 *Braz. J. Phys.* **3B** 994
[3] Wang H, Zhang S, Li Y and Sun D 2008 *Thin Solid Films* **516** 5419

[4] Dudek M, Amassian A, Zabeida O, Klemberg-Sapieha J E and Martinu L 2009 *Thin Solid Films* **517** 4576
[5] Jun S I, Rackv P D, McKnight T E, Melechko A V and Simpson M L 2005 *Appl. Phys. Lett.* **87** 132108
[6] Shakhnazarov K Y and Shakhnazarov A Y 2001 *Met. Sci. Heat Treat.* **43** 431
[7] Huang P K and Yeh J W 2009 *J. Phys. D: Appl. Phys.* **42** 115401
[8] Chapman B 1976 *Glow Discharge Processes: Sputtering and Plasma Etching* (New York: Wiley) chapter 6 p 216
[9] Larijani M M, Elmi M, Yari M, Ghoranneviss M, Balashabadi P and Shokouhy A 2009 *Surf. Coat. Technol.* **203** 2591
[10] Abe K, Harada Y and Onoda H 1998 *Proc. 36th IEEE Int. Reliability Physics Symp. (Reno, NV)* pp 342–7
[11] Chen C S, Liu C P, Yang H G and Tsao C Y A 2004 *J. Vac. Sci. Technol.* B **22** 1075
[12] Signore M A, Rizzo A, Mirenghi L, Tagliente M A and Cappello A 2007 *Thin Solid Films* **515** 6798
[13] 2000 *JCPDS—International Centre for Diffraction Data* Copyright (C) JCPD-ICDD
[14] Birkholz M 2006 *Thin Film Analysis by X-ray Scattering* (Weinheim: Wiley)
[15] Boxman R L, Zhitomirsky V N, Grimberg I, Rapoport L, Goldsmith S and Weiss B Z 2000 *Surf. Coat. Technol.* **125** 257
[16] Pilloud D, Dehlinger A S, Pierson J F, Roman A and Pichon L 2003 *Surf. Coat. Technol.* **174–175** 338
[17] Schlegel A, Wachter P, Nickl J J and Lingg H 1977 *J. Phys. C: Solid State Phys.* **10** 4889
[18] Wang C C, Akbar S A, Chen W and Patton V D 1995 *J. Mater. Sci.* **30** 1627
[19] Bhuvaneswari B, Priya I N, Chandramani R, Reddy V R and Rao G M 2003 *Cryst. Res. Technol.* **38** 1047
[20] Straboni A, Pichon L and Girardeau T 2000 *Surf. Coat. Technol.* **125** 100
[21] Bubenzer A, Dischler B, Brandt G and Koidl P 1983 *J. Appl. Phys.* **54** 4590
[22] Zhang Y J, Yan P X, Wu Z G, Zhang W W, Zhang G A, Liu W M and Xue Q J 2005 *Phys. Status Solidi* a **202** 95
[23] Hultman L, Sundgren J E and Greene J E 1995 *J. Appl. Phys.* **78** 5395
[24] Ashok K, Subramanian B, Kuppusami P and Jayachandran M 2009 *Cryst. Res. Technol.* **44** 511
[25] Arias F, Arango Y C and Devia A 2006 *Appl. Surf. Sci.* **253** 1683
[26] Glew M R L, Vollmer A, Schroeder S L M and Barber Z H 2002 *J. Phys. D: Appl. Phys.* **35** 2643
[27] Lavrenko V A, Shvets V A, Panasyuk A D and Kuznetsova L I 2003 *Powder Metall. Met. Ceram.* **42** 419
[28] Huang J H, Chang K H and Yu G P 2007 *Surf. Coat. Technol.* **201** 6404
[29] Petrov I, Hultman L, Helmersson U, Sundgren J E and Greene J E 1989 *Thin Solid Films* **169** 299
[30] Benia H M, Guemmaz M, Schmerber G, Mosser A and Parlebas J C 2002 *Appl. Surf. Sci.* **200** 231